Suppressing Short-Term Polarization Noise and Related Spectral Decoherence in All-Normal Dispersion Fiber Supercontinuum Generation

Yuan Liu, Youbo Zhao, Jens Lyngsø, Sixian You, William L. Wilson, Haohua Tu, and Stephen A. Boppart, *Fellow, IEEE*

***Abstract*—The supercontinuum generated exclusively in the normal dispersion regime of a nonlinear fiber is widely believed to possess low optical noise and high spectral coherence. The recent development of flattened all-normal dispersion fibers has been motivated by this belief to construct a general-purpose broadband coherent optical source. Somewhat surprisingly, we identify a large short-term polarization noise in this type of supercontinuum generation that has been masked by the total-intensity measurement in the past, but can be easily detected by filtering the supercontinuum with a linear polarizer. Fortunately, this hidden intrinsic noise and the accompanied spectral decoherence can be effectively suppressed by using a polarization-maintaining all-normal dispersion fiber. A polarization-maintaining coherent supercontinuum laser is thus built with a broad bandwidth (780–1300 nm) and high spectral power (∼1 mW/nm).**

***Index Terms*—Fiber nonlinear optics, laser noise, optical pulse compression, supercontinuum generation.**

I. Introduction

SUPERCONTINUUM (SC) generation was first observed in a normally dispersive bulk glass where mJ-level ps green input pulses acquired dramatic spectral broadening to become white light [1]. In 1987, this effect was realized in an optical fiber using μJ-level 50-fs red pulses, while the single-mode output was compressed into near transform-limited 6-fs pulses [2]. Because the spectral broadening occurs exclusively in the normal dispersion regime of the fiber, this all-normal dispersion (ANDi) SC generation avoids unstable soliton dynamics and/or modulation instability prevalent in the anomalous dispersion regime [3]. Thus, the input quantum noise is not amplified, i.e., the spectral decoherence is not accumulated to disrupt high-quality pulse compression [4]. Inspired by the 1999 innovation of hybrid anomalous-normal dispersion (HANDi) fiber SC generation that has enabled wide access to ultra-broadband laser-like sources [5], recently revived efforts in the ANDi fiber SC generation have claimed to develop various low-noise coherent SC sources by coupling common nJ-level ∼100 fs input pulses into dispersion-flattened Ge-doped circular fibers [6], pure-silica photonic crystal fibers [7]–[9], and soft-glass all-solid microstructured fibers [10]. Octave-spanning bandwidth has been attained to center at 1550 nm [6], [10], 1050 nm [7], [8], and 800 nm [8]. The low optical noise has been confirmed by relative intensity noise (RIN) measurements [6] and ultrafast transient absorption spectroscopy [8], while the high coherence by spectral interference [6] and pulse compression [7], [9]. These experiments are highly consistent with theoretical analysis [11], reinforcing the general notion that the ANDi fiber SC sources are not limited by optical noise or decoherence [4]. Rather unexpectedly, here we identify a noise/decoherence mechanism in these sources that have universally employed non-polarization-maintaining fibers with weak unintentional birefringence ($< 10^{-4}$).

The unintentional latent birefringence of these nonlinear fibers, although small, defines a distinct slow axis along which linearly polarized SC output can be produced when a polarized input is launched along this axis, i.e., the SC generation can be effectively polarization-maintaining [12]. However, above a certain threshold of output power, this SC suffers a hardly controllable nonlinear depolarization effect [12]–[14], so that the spectrum of the SC defies the scalar generalized nonlinear Schrödinger equation (GNLSE) [13] and the polarization of the SC endures long-term (<100 Hz) instability of thermal origin instability [14]. In these prior works, the depolarization effect has been attributed to vector modulation instability [3], [15]. Importantly, the observed long-term (<100 Hz) instability [14] should be discriminated against short-term (>1 MHz) RIN noise [6], because the later corresponds to the intrinsic (quantum) broadband noise component due to input shot noise and spontaneous Raman scattering, while the former the large-amplitude noise component at low frequencies that results from technical noise [4]. The noise discussed throughout this study corresponds to the short-term optical *noise*, rather than the long-term *instability*.

It is then unclear whether vector modulation instability induces short-term intrinsic noise and spectral decoherence during the ANDi fiber SC generation, just like scalar modulation instability does during ps HANDi fiber SC generation [4]. In this study, we directly observe the short-term noise by polarized RIN measurements and the spectral decoherence through pulse compressibility assessment. Thus, the nonlinear depolarization

Manuscript received October 8, 2014; revised January 14, 2015; accepted January 25, 2015. Date of publication January 26, 2015; date of current version March 13, 2015. This work was supported in part by the National Institutes of Health under Grants R01 CA166309 and R01 EB013723.

Y. Liu, Y. Zhao, S. You, H. Tu, and S. A. Boppart are with the Biophotonics Imaging Laboratory, University of Illinois at Urbana-Champaign, Urbana, IL 61801 USA (e-mail: yuanliu3@illinois.edu; ybzhao@illinois.edu; syou10@illinois.edu; htu@illinois.edu; boppart@illinois.edu).

J. Lyngsø is with the NKT Photonics A/S, 3460 Birkerød, Denmark (e-mail: jkl@nktphotonics.com).

W. L. Wilson is with the Materials Research Laboratory, University of Illinois at Urbana-Champaign, Urbana, IL 61801 USA (e-mail: wlwilson@illinois.edu).

Color versions of one or more of the figures in this papers are available online at http://ieeexplore.ieee.org.

Digital Object Identifier 10.1109/JLT.2015.2397276

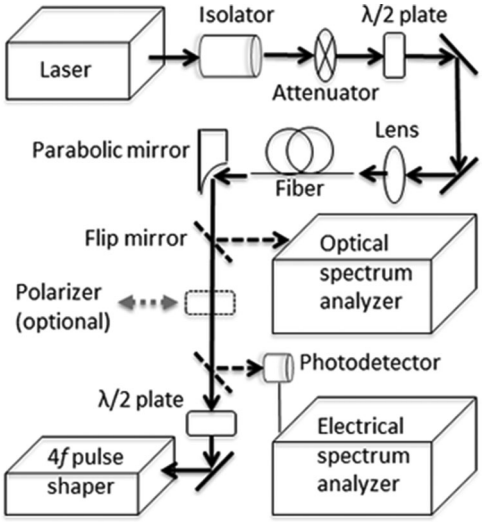

Fig. 1. A schematic of SC generation and characterization. An optional linear polarizer is inserted to measure the RIN of polarizer-filtered SC and compress the SC pulse, or removed to measure the RIN of unfiltered SC.

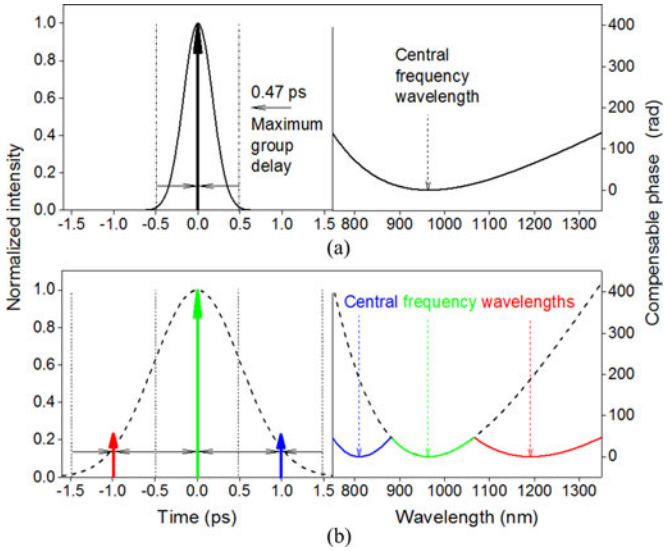

Fig. 2. (Color online). Global compression (a) versus 3-segment local compression (b) of a linearly chirped broadband (750–1350 nm) pulse at the times of central frequency wavelengths (vertical arrows in the time domain). The finite spectral resolution of the 640-pixel 4f pulse shaper (0.94 nm/pixel) allows a much larger compensable phase in the local compression than the global compression (broken and solid black curves in the spectral domain), and thus limits the dynamic range to 3 pairs of maximum group delays in the local compression, rather than only one pair of maximum group delays in the global compression (horizontal arrows in the time domain).

and vector modulation instability not only negatively affect the controllability and long-term stability of the ANDi fiber SC generation [13], [14], but also fundamentally limit the application of this technology when full spectral coherence or low-noise polarized source is required. By fabricating a dispersion-flattened ANDi photonic crystal fiber with a large intentional birefringence ($>10^{-4}$), we suppress these effects and therefore develop a high-power broadband coherent SC laser.

II. Methods

The experimental setup adopted our reported apparatus [12], [13] to couple linearly polarized (>500 polarization extinction ratio) 1041-nm ~80-MHz 229-fs sech^2 pulses into a nonlinear photonic crystal fiber of 9–40 cm length (Fig. 1). Different focusing aspheric lenses might be used for different nonlinear fibers (see below) to ensure a coupling efficiency of >60%. The generated SC was collimated by a gold-coated parabolic mirror so that its spectrum could be accurately measured by an optical spectrum analyzer. The RIN measurements on the SC were performed according to an established method [16], using a broadband (700–1800 nm) fast (10 ns rise time) InGaAs photodetector (DET10C, Thorlabs, Inc.) connected to an electrical spectrum analyzer (HP 8561E, Agilent). To compare the RIN from different SC sources, care was taken to ensure that the same power (~1 mW) was incident on the photodetector below its saturation limit [16].

The horizontally polarized SC required for subsequent pulse compression was enforced by a broadband polarizer and an achromatic half-wave plate after the fiber (Fig. 1). The pulse compression was conducted by a 640-pixel 4f pulse shaper (MIIPSBox 640, BioPhotonic Solutions Inc.), which employed the pulse measurement of multiphoton intrapulse interference phase scans (MIIPS) [17], [18] to iteratively compress the SC pulse [9], [19]. Alternative pulse measurements based on FROG [20] and SPIDER [21], [22] have also enabled the iterative compression of other fiber SC pulses by similar 4f pulse shapers. The coherence of the SC can be validated if converged iteration toward transform-limited pulse compression is demonstrated [9], [19]–[22].

The common limitation of these pixelated 4f pulse shaper-based pulse compressions is the finite spectral resolution or (temporal) dynamic range [23]. The design of our pulse shaper covers a bandwidth $\Delta\lambda$ from 750 nm (λ_1) to 1350 nm (λ_2), corresponding to a spectral resolution of 0.94 nm/pixel ($\delta\lambda$). Because high-fidelity pulse generation and compression restrict the spectral phase variation between adjacent pixels to within $\pi/2(\delta\phi)$, the spectral phase variation at λ_1 dictates a maximum group delay $\delta\phi/\delta\omega$ [i.e., $\delta\phi/(2\pi c\delta\lambda/\lambda_1^2)$] of 0.47 ps, i.e., a dynamic range of 0.94 ps for a linearly chirped pulse (Fig. 2(a)). Equivalently, a broadband (750–1350 nm) linearly chirped pulse can be "globally" compressed at the time of its central frequency wavelength $(1/\lambda_1 + 1/\lambda_2)^{-1}$ (Fig. 2(a), vertical arrow in the time domain) only if the pulse duration is less than 0.94 ps. Thus, a broadband (750–1350 nm) linearly chirped pulse with 3×0.94 ps duration cannot be "globally" compressed at the time of its central frequency wavelength. However, if the bandwidth is divided into 3 segments of equal optical frequency range, each segment can then be "locally" compressed to the time of its own central frequency wavelength within the limit of adjacent-pixel phase variation (Fig. 2(b), colored vertical arrows in the time domain) [24]. In other words, the local compression of the spectral segments expands the dynamic range of the pulse shaper without affecting the coherence assessment, as long as the converged iteration toward transform-limited pulse compression can be demonstrated for

all segments. In this study, 10-segment local compression with an expanded dynamic range of 10×0.94 ps was used to accommodate the large linear chirp of our fiber SC pulses. The spectral components outside of the intended segment for local compression were simply blocked by amplitude shaping [19].

III. Results

To establish a baseline for SC generation and characterization, the specific SC from an ANDi photonic crystal fiber (NL-1050-NEG-1, NKT Photonics, Denmark) is reproduced (Fig. 3(a)) [9], [12], [13]. With an unintentional linear birefringence on the order of 10^{-5}, the slow and fast axes of a 9-cm fiber can be easily identified [12]. The SC is then generated at 360 mW output power using a slow-axis input, with a spectrum that can be quantified by the scalar GNLSE (Fig. 3(a), (b)). Using a broadband polarizer at the fiber exit end to filter the SC along the slow-axis (Fig. 1), a nonlinear depolarization of only 4% is obtained, i.e., 96% power of the SC output remains along the slow-axis [13]. The local compression is successfully demonstrated to validate the high coherence of the polarized slow-axis-filtered SC, consistent with the demonstrated global compression [9]. Not surprisingly, at Fourier frequencies around the carrier frequency of the input laser (80.2 MHz), the RIN of either the filtered SC or the unfiltered SC (without the polarizer) can be barely detected beyond that of the solid state input laser or the noise floor of our detection system (Fig. 4(a)). These results agree well with the general consensus that ANDi fiber SC generation has low optical noise and high spectral coherence [2], [4], [6]–[11].

However, in attempts to produce a broader coherent bandwidth, dramatically different results are obtained from a longer fiber of 21 cm at a higher output power of 480 mW. A large nonlinear depolarization of 50% is encountered, so that the measured SC spectrum (Fig. 3(d)) differs significantly from the corresponding scalar-GNLSE prediction (Fig. 3(e)). A broadband high-frequency (short-term) RIN of 30.8 dB emerges from the noise floor for the slow-axis-filtered SC (Fig. 4(b)), indicating the presence of intrinsic noise with quantum origin [4]. At the same time, the filtered SC fails the local compression test, i.e., the iterative compression does not converge to retrieve a deterministic spectral phase for each segment, even though the GNLSE-predicted pulse width of the SC (Fig. 3(e), inset) is well within the temporal dynamic range of the local compression. In other words, the ANDi SC generation suffers a noise/decoherence mechanism as a result of the nonlinear depolarization. Because a near constant filtered power is obtained by rotating the polarizer (Fig. 1), the depolarization appears to be uniform among all linear polarization orientations. While the same level of RIN can be measured from the SC filtered along the fast axis, much smaller RIN (5.6 dB) is attained when the polarizer is oriented at 45° between the slow and fast axes (Fig. 4(b)). Interestingly, no RIN can be detected from the unfiltered SC if the polarizer is removed (Fig. 4(b)). This total-intensity RIN remains undetectably low when longer fiber lengths (up to 40 cm) and/or higher output powers (up to 700 mW) are used.

The nonlinear depolarization, along with the three accompanied effects (i.e., modeling error by scalar GNLSE, RIN onset in polarizer filtered SC but not unfiltered SC, and spectral decoherence of the filtered SC), can be observed under a wide variety of conditions that broaden the bandwidth beyond 900–1160 nm (Fig. 3(a)). For example, similar SC spectrum to Fig. 3(d) and large depolarization (50%) can be observed at 360 mW output power from a 40 cm fiber. Using fiber cut-backs from 40 cm to 9 cm, the depolarization and the RIN of the slow-axis-filtered

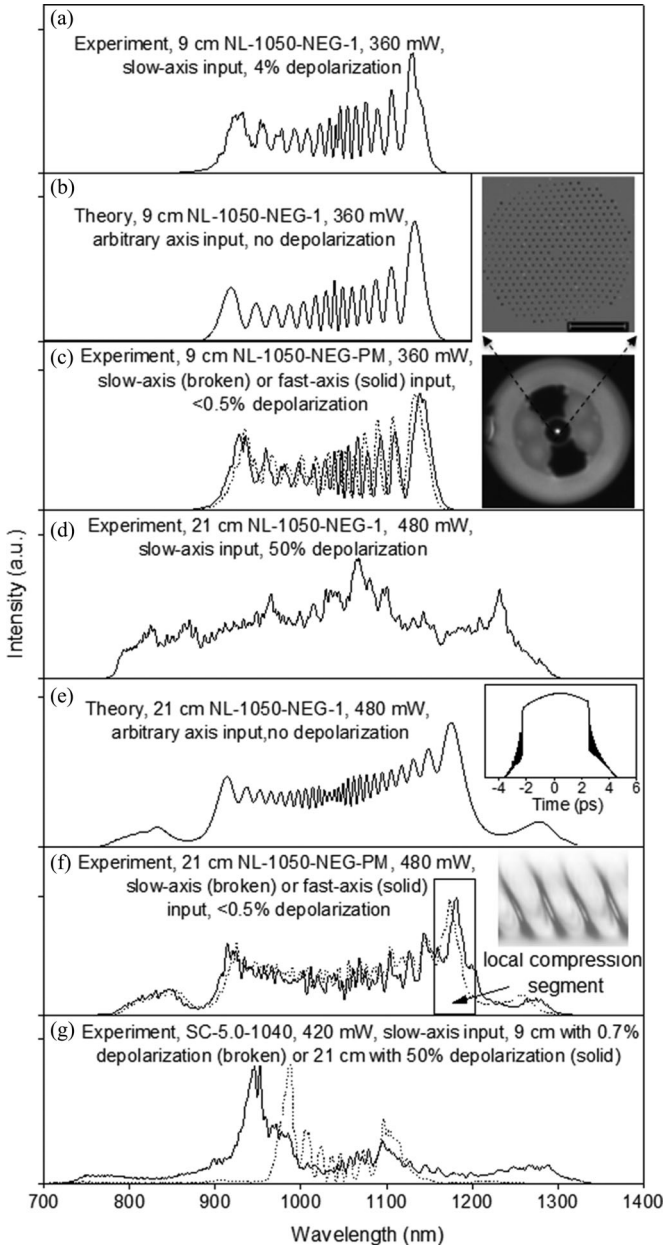

Fig. 3. Experimental spectra and scalar-GNLSE quantified spectra for SC sources. The comparison of (a)–(c) with (d)–(f) indicates that the observed spectrum from either a non-polarization-maintaining fiber or its polarization-maintaining counterpart can be theoretically quantified in relatively narrowband (900–1160 nm) SC generation. However, in broadband (780–1300 nm) SC generation, only the later can be theoretically quantified due to the absence of depolarization. Insets in (c): cross-sectional optical (lower) and scanning electron microscopy (upper, scale bar 10 μm) images of the polarization-maintaining fiber; inset in (e): temporal profile of SC pulse; inset in (f): characteristic MIIPS trace of a local compression segment indicative of transform-limited pulse compression [9], [17]–[19].

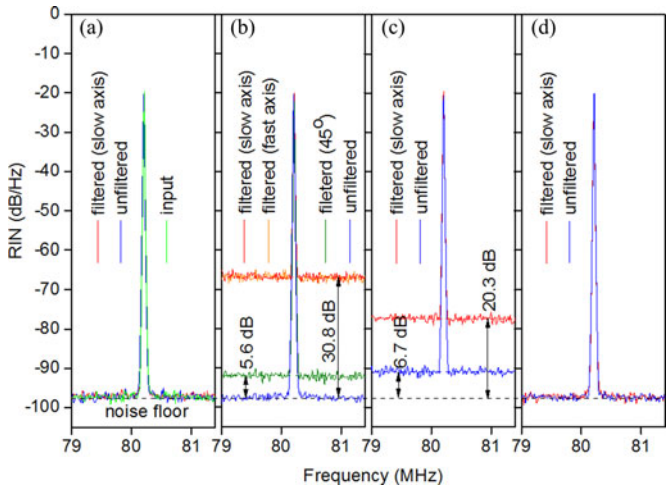

Fig. 4. (Color online). RIN (10 kHz resolution bandwidth) measured from four SC sources with a slow-axis input. (a) 9-cm NL-1050-NEG-1, 360 mW output, 3% depolarization; (b) 21-cm NL-1050-NEG-1, 480 mW output, 50% depolarization; (c) 21-cm SC-5.0–1040, 420 mW output, 50% depolarization; and (d) 21-cm NL-1050-NEG-PM, 480 mW output, $<0.5\%$ depolarization. Broken black line represents the noise floor without incident light. The same height of RIN (-20 dB) at the carrier frequency (i.e., repetition rate of input laser, 80.2 MHz) ensures equal incident power on the photodetector.

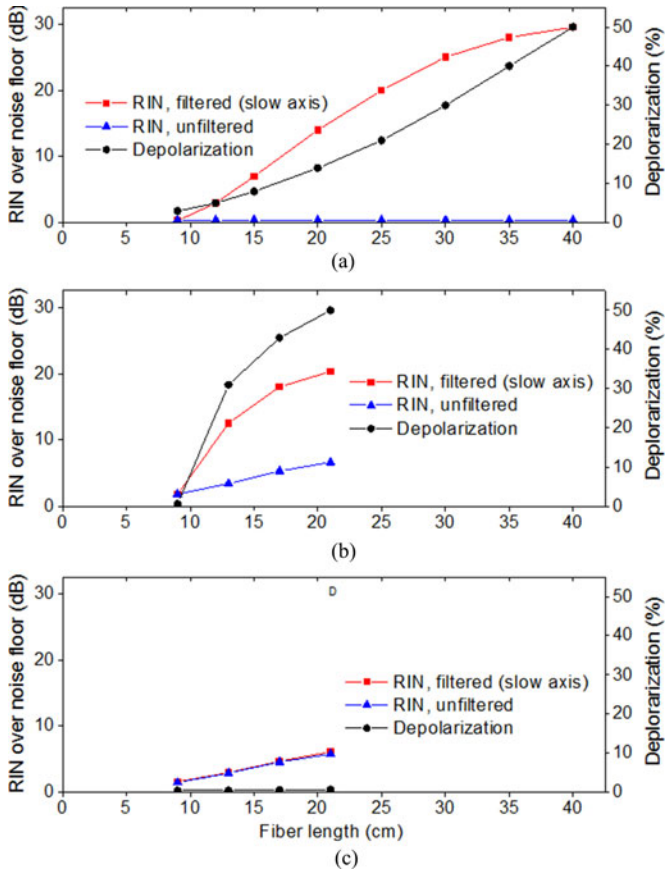

Fig. 5. (Color online). RIN (10-kHz resolution bandwidth) measured from three SC sources with a slow-axis input, with the dependence on the fiber length determined by fiber cut-backs. (a) NL-1050-NEG-1, 360 mW output, 40 cm initial length; (b) SC-5.0–1040, 420 mW output, 21 cm initial length; and (c) SC-5.0–1040-PM, 420 mW output, 21 cm initial length.

SC are measured along the fiber length (Fig. 5(a)). The synchronized decrease of the depolarization and RIN with shortened fiber length suggests that the two effects are correlated, and may occur right at the entrance end of the fiber (i.e., the RIN is amplified from certain input shot noise). After the cutbacks, the shortened fiber with 9-cm length expectedly recovers the baseline condition (Fig. 3(a), Fig. 4(a)).

A natural question arises how the ANDi fiber SC generation compares with the more popular alternative of HANDi fiber SC generation in terms of noise and decoherence. To enable the comparison, a photonic crystal fiber with zero-dispersion wavelength of 1040 nm (SC-5.0–1040, NKT Photonics, Denmark) is selected for the HANDi SC generation. Similar fibers have been employed in commercial SC laser developments [25], [26]. The unintentional linear birefringence is on the order of 10^{-6}, which is adequate to identify the slow and fast axes of a 21-cm fiber [12], [13]. Given a slow-axis input, the SC is generated at 420 mW output power to obtain a bandwidth (Fig. 3(g)) comparable to that of the ANDi fiber SC (Fig. 3(d)), with a depolarization of 50% along the slow-axis (Fig. 5(b)). Similar to the ANDi fiber SC (Fig. 4(b)), considerable RIN (20.3 dB) can be detected from this SC filtered along the slow-axis (Fig. 4(c)), so that it fails the local compression test. However, in sharp contrast to the ANDi fiber SC, significant total-intensity RIN (6.7 dB) is retained when the polarizer is removed (Fig. 4(c)). A similar cutback experiment is conducted on this fiber from 21 cm to 9 cm, showing the accumulation of the depolarization and RIN along the fiber (Fig. 5(b)). At 9 cm fiber length, the depolarization is negligibly small (0.7%), while the RIN of the slow-axis-filtered SC (1.9 ± 0.3 dB) approximates that of the unfiltered SC (1.9 ± 0.3 dB) (Fig. 5(b)). The emergence of this total-intensity RIN free of appreciable depolarization leads to the failed local compression test for the slow-axis-filtered SC.

To evaluate how the birefringence of the fiber affects the HANDi SC generation, a polarization-maintaining equivalent of SC-5.0–1040 (SC-5.0–1040-PM, NKT Photonics, Denmark) is also investigated. The large intentional birefringence of this fiber ($> 1.7 \times 10^{-4}$) ensures linearly polarized SC generation if the input polarization is aligned with the slow-axis or the fast-axis. A similar cutback experiment is performed on a 21-cm fiber with slow-axis input and 420 mW output (Fig. 5(c)). The accumulation of the total intensity RIN along the fiber is similar to the non-polarization-maintaining case in Fig. 5(b), while the spectral broadening of the polarization-maintaining SC along the fiber approximates that of the progressively depolarized SC in Fig. 3(g). Because $>99.5\%$ of SC power stays in the slow axis, the RIN of the slow-axis-filtered SC differs little from that of the unfiltered SC (Fig. 5(c)).

IV. Discussion

To interpret the above results, we differentiate two fundamentally different coherence-disrupting noises integrated over the full SC bandwidth: (1) pulse-energy-fluctuated total-intensity noise specific to the HANDi fiber SC generation; and (2) pulse-energy-conserved polarization noise specific to the ANDi fiber SC generation. While it is outside the scope of this study to

perform quantitative analysis on these noise sources, we show below that a simple qualitative understanding using this differentiation offers two practical strategies to independently suppress the two noise sources, even though they both are quantum noise sources in nature.

The total-intensity noise is clearly revealed in the polarization-maintaining HANDi fiber SC generation (Fig. 5(c)). The presence of large RIN (variation) among spectrally filtered narrowband ($\sim$10 nm) components across the SC have been observed with fs [27] or ps input [28]. However, this spectral RIN does not necessarily lead to the observed total-intensity noise integrated over the full SC bandwidth. The simplest explanation to the total-intensity noise is through rogue-wave-like characteristics, discovered first in ps SC generation [29] and extended later to fs SC generation [30]. Specifically, a generated SC pulse is mostly "median" so that its long-wavelength edge solitons undergo average redshifts, resulting in a normal energy loss to the pulse. However, the SC pulse may occasionally be "rogue" so that its long-wavelength edge solitons undergo stronger redshifts, resulting in a larger energy loss to the pulse. This pulse-to-pulse energy fluctuation is more pronounced in a longer fiber where the disparity of the redshifts is enlarged [31], leading to the observed buildup of total-intensity noise along the fiber (Fig. 5(c)).

The polarization noise is revealed in the depolarized ANDi fiber SC generation by the RIN of the slow-axis-filtered SC in excess to that of the unfiltered SC (Fig. 5(c)). The unusually large RIN (30.8 dB) observed along either the slow or fast axis indicates a large pulse-to-pulse energy fluctuation along this axis (Fig. 4(b)). The much smaller RIN (5.6 dB) observed along the 45°-axis suggests a cancelled pulse-to-pulse fluctuation to the corresponding pulse energy, which has one half contribution from the slow axis and the other half from the fast axis. That is, the gain (loss) of the pulse energy along the slow axis is always cancelled by the loss (gain) of the pulse energy along the fast axis, so that the total pulse energy is conserved. The RIN along the 45°-axis does not fall on the noise floor to approximate that of the unfiltered SC (Fig. 4(b)), i.e., the cancellation is not perfect. This is likely due to the twist of the fiber, which superimposes a small circular birefringence to the unintentional linear birefringence. The resulting elliptical birefringence modifies the orthonormal decomposition of the pulse field from a pair of orthogonal linear directions to a pair of elliptically polarized directions, leading to the imperfect noise cancelation by the linear polarizer [3]. Nevertheless, the total pulse energy is conserved if the coupled GNLSE would be performed on the elliptically birefringent fiber in the rogue-wave-free ANDi SC generation [3]. Because the polarization-dependent dispersion elements of pulse compression experiments demand a single-polarization input, the noisy polarizer-filtered SC (rather than the quiet unfiltered SC) must be used in the local compression test. The test fails as a result of the large polarization noise, which apparently introduces phase noise to disrupt the spectral coherence of the SC.

This polarization noise eluded detection in the past when only total-intensity measurements were conducted [6], [8]. An early theoretical study on depolarized fiber SC generation [32], which used a semi-classical model of input noise in a single polarization [4], concluded that the ANDi fiber SC generation should have both high polarization stability and excellent coherence. We speculate that the observed polarization noise can only be predicted after the semi-classical noise model is modified to include input noise along two orthonormal polarizations. Because the simulated SC generation above an output power threshold is sensitive to (instable against) the input polarization [13], the observed polarization noise may arise from the amplification of the input shot noise that distributes photons along the two orthonormal polarizations. The amplification gain is likely attributed to the vector modulation instability [13], just like the single-polarization noise amplification in ps HANDi fiber SC generation can be attributed to scalar modulation instability [4].

More complex situation is encountered in the depolarized HANDi fiber SC generation (Fig. 5(b)), where the observed noise is a mixture of the total-intensity noise and polarization noise. Similar result has also been attained in a recent study [33]. We caution that the widely used scalar GNLSE noise models have ignored the polarization noise [4], [34], and are therefore approximate whenever the SC generation is not polarization-maintaining. On the other hand, the total-intensity noise can be considered as a more fundamental noise than the polarization noise. First, the mixed noise does not conserve the pulse energy, just like the total-intensity noise (compare Fig. 5(b) with (c)). Second, the total-intensity noise buildups more quickly than the polarization noise, and thus dominates the noise at short ($<$9 cm) fiber lengths (Fig. 5(b)). Third, the polarization noise can be eliminated by simply using a polarization-maintaining fiber (compare Fig. 5(b) with (c)), while the total-intensity noise can only be decreased by more complicated techniques, such as sliding frequency filter [31], input envelope modulation [35], minute light seeding [36], back seeding [37], and fiber tapering [38].

V. Polarization-Maintaining Fiber Coherent SC Laser

Suggested by the above discussions, we adopt two strategies in order to build a broadband coherent fiber SC laser. First, the coherence-disrupting total-intensity noise is avoided by the ANDi fiber SC generation free of the rogue behavior. Second, the coherence-disrupting polarization noise is eliminated by the use of a polarization-maintaining fiber with large intentional linear birefringence. In combination, this laser relies on the ANDi fiber SC generation from a polarization-maintaining fiber.

We thus fabricate the polarization-maintaining counterpart of NL-1050-NEG-1 (NL-1050-NEG-PM) by introducing stress rods in the fiber cladding (Fig. 3(c), inset). The cross section parameters of the fabricated fiber (hole-to-hole pitch, hole size, and number of layers, see [12]) approximate those of NL-1050-NEG-1, so that the dispersion properties of the two fibers are comparable. Consistently, the 360-mW SC generated from a 9-cm NL-1050-NEG-PM fiber with a fast-axis (or slow-axis) input (Fig. 3(c)) approximates that from the NL-1050-NEG-1 fiber (Fig. 3(a)) and the corresponding simulation (Fig. 3(b)). The linear birefringence of the fiber is estimated to be 4.2×10^{-4} by spectral interferometry, ensuing no detectable nonlinear depolarization along either axis.

In sharp contrast to the non-polarization-maintaining case (Fig. 3(d)), little depolarization ($<0.5\%$) is found in the 480-mW SC generated from a 21-cm NL-1050-NEG-PM fiber with a fast-axis (or slow-axis) input. The spectrum of the polarization-maintaining SC agrees well with the simulated spectrum (Fig. 3(e), (f)), as the two wave-breaking-related sidelobes at the short- and long-wavelength ends become distinguishable from the central self-phase modulation features [39]. No RIN can be detected from this SC (Fig. 4(d)), while the local compression test succeeds for any arbitrarily selected 50-nm segment inside the SC bandwidth (Fig. 3(f), inset), i.e., the SC recovers full spectral coherence. With the simultaneous disappearance of the three undesirable effects accompanying the depolarization, the polarization-maintaining fiber significantly improves the coherent bandwidth and output power over its non-polarization-maintaining predecessor. The potentially large but unintentional birefringence of the later may occasionally generate a broad coherent bandwidth [39], but this has not been reproducible among different fiber pieces. Throughout a one-year test on the polarization-maintaining fiber, the SC spectrum of Fig. 3(f) has been reproducibly attained in daily operations, not only from one fiber piece but also from other 21-cm fiber pieces. Longer fiber lengths and larger output powers only marginally broaden the bandwidth. To further broaden the bandwidth beyond 780–1300 nm, a dechirped transform-limited input pulse [12] with shorter pulse width [8], [11] will be employed in the near future.

To put the above polarization-maintaining fiber coherent SC laser into a broad context, we examine a series of octave-spanning ANDi fiber SCs developed recently [6]–[8], [10]. Because the corresponding nonlinear fibers have no intentional birefringence, these SCs presumably undergo the same nonlinear depolarization, and therefore accumulate large polarization noise and spectral decoherence. It should be noted that the agreement of the observed log-scale SC spectrum with that simulated by the scalar GNLSE is not sufficient to confirm the coherence of the SC [8]. The observed spectrum of the depolarized SC (Fig. 3(d)) is rather similar to that of the polarization-maintaining SC (Fig. 3(f)) and the simulated SC (Fig. 3(e)), if all three were plotted in a log-scale. Also, the reported low RIN [6] and temporal fluctuation [8] are based on total intensity measurements [6], which mask the detection of the polarization noise as discussed above. Finally, the interference experiment to confirm the spectral coherence of the SC would be convincing if the similarly measured HANDi fiber SC had not exhibited a high degree of coherence (~ 0.7) [6]. Up to now, there has been no definitive evidence supporting that these octave-spanning sources are low-noise coherent sources.

VI. Conclusion

We identify a latent short-term polarization noise in the ANDi fiber SC generation, which redistributes the SC pulse energy pulse-by-pulse along the slow and fast axes, but conserves the total pulse energy. This noise is fundamentally different from the total-intensity noise in the HANDi fiber SC generation that does not conserves the total pulse energy pulse-by-pulse. Thus, the absence of the total-intensity noise distinctly separates the ANDi fiber SC generation from the HANDi fiber SC generation. However, this absence does not guarantee high-quality pulse compression pertinent to single-polarization coherent applications, because the polarization noise causes spectral decoherence just like the total-intensity noise. In fact, under certain conditions, the ANDi fiber SC may be noisier than the HANDi fiber SC with a similar bandwidth (compare Fig. 4(b) and (c)). By fabricating a polarization-maintaining ANDi fiber, we completely suppress the polarization noise and thus develop a polarization-maintaining fiber coherent SC laser with a broad bandwidth and high output power.

We would like to point out some unusual similarities between the observed short-term (>1 MHz) polarization noise and the reported long-term (<100 Hz) polarization instability [14]: (1) both occur above certain power thresholds below which the effects simply disappear; (2) both redistribute the transmission power along two principal fiber axes but conserve the total power, so that the effects are masked by total intensity measurements; (3) both occur in fibers with latent birefringence, and can be fully suppressed when polarization-maintaining fibers are used. It is an extraordinary coincidence that the same effects happen at two dramatically different timescales but may be the result from the same underlining mechanism of vector modulation instability [15].

The observed polarization noise of the SC is likely seeded by the input shot noise that stochastically distributed the input photons along two orthonormal polarization directions. The presence of this noise in the popular HANDi fiber SC generation calls for a new vector GNLSE noise model that takes account of the input polarization noise and the unintentional (linear and circular) birefringence of the fiber. In the depolarized ANDi fiber SC generation, the SC is quiet in total intensity, but noisy in two orthogonally polarized components. This unique property is worth further theoretical studies, and may be useful in some polarization-dependent applications.

Acknowledgment

The authors would like to thank Darold Spillman for his technical support.

References

[1] R. R. Alfano and S. L. Shapiro, "Emission in the region 4000 to 7000 Å via four-photon coupling in glass," *Phys. Rev. Lett.*, vol. 24, pp. 584–587, Mar. 1970.

[2] R. L. Fork, C. H. Cruz, P. C. Becker, and C. V. Shank, "Compression of optical pulses to six femtoseconds by using cubic phase compensation," *Opt. Lett.*, vol. 12, pp. 483–485, Jul. 1987.

[3] G. P. Agrawal, "Chapter 5 optical solitons and chapter 6 polarization effects," in *Nonlinear Fiber Optics*. San Francisco, CA, USA: Academic, 2007, pp. 120–225.

[4] J. M. Dudley, G. Genty, and S. Coen, "Supercontinuum generation in photonic crystal fiber," *Rev. Mod. Phys.*, vol. 78, pp. 1135–1184, Oct. 2006.

[5] J. K. Ranka, R. S. Windeler, and A. J. Stentz, "Visible continuum generation in air-silica microstructure optical fibers with anomalous dispersion at 800 nm," *Opt. Lett.*, vol. 25, pp. 25–27, Jan. 2000.

[6] N. Nishizawa and J. Takayanagi, "Octave spanning high-quality supercontinuum generation in all-fiber system," *J. Opt. Soc. Am. B*, vol. 24, pp. 1786–1792, Aug. 2007.

[7] L. E. Hooper, P. J. Mosley, A. C. Muir, W. J. Wadsworth, and J. C. Knight, "Coherent supercontinuum generation in photonic crystal fiber with all-normal group velocity dispersion," *Opt. Exp.*, vol. 19, pp. 4902–4907, Mar. 2011.
[8] A. M. Heidt, A. Hartung, G. W. Bosman, P. Krok, E. G. Rohwer, H. Schwoerer, and H. Bartelt, "Coherent octave spanning near-infrared and visible supercontinuum generation in all-normal dispersion photonic crystal fibers," *Opt. Exp.*, vol. 19, pp. 3775–3787, Feb. 2011.
[9] H. Tu, Y. Liu, J. Lægsgaard, D. Turchinovich, M. Siegel, D. Kopf, H. Li, T. Gunaratne, and S. A. Boppart, "Cross-validation of theoretically quantified fiber continuum generation and absolute pulse measurement by MIIPS for a broadband coherently controlled optical source," *Appl. Phys. B*, vol. 106, pp. 379–384, Feb. 2012.
[10] M. Klimczak, B. Siwicki, P. Skibiński, D. Pysz, R. Stępień, A. Heidt, C. Radzewicz, and R. Buczyński, "Coherent supercontinuum generation up to 2.3 μm in all-solid soft-glass photonic crystal fibers with flat all-normal dispersion," *Opt. Exp.*, vol. 22, pp. 18824–18832, Jul. 2014.
[11] A. M. Heidt, "Pulse preserving flat-top supercontinuum generation in all-normal dispersion photonic crystal fibers," *J. Opt. Soc. Am. B*, vol. 27, pp. 550–559, Mar. 2010.
[12] H. Tu, Y. Liu, J. Lægsgaard, U. Sharma, M. Siegel, D. Kopf, and S. A. Boppart, "Scalar generalized nonlinear Schrödinger equation-quantified continuum generation in an all-normal dispersion photonic crystal fiber for broadband coherent optical sources," *Opt. Exp.*, vol. 18, pp. 27872–27884, Dec. 2010.
[13] H. Tu, Y. Liu, X. Liu, D. Turchinovich, J. Lægsgaard, and S. A. Boppart, "Nonlinear polarization dynamics in a weakly birefringent all-normal dispersion photonic crystal fiber: Toward a practical coherent fiber supercontinuum laser," *Opt. Exp.*, vol. 20, pp. 1113–1128, Jan. 2012.
[14] S. R. Domingue and R. A. Bartels, "Overcoming temporal polarization instabilities from the latent birefringence in all-normal dispersion, wave-breaking-extended nonlinear fiber supercontinuum generation," *Opt. Exp.*, vol. 21, pp. 13305–13321, Jun. 2013.
[15] S. G. Murdoch, R. Leonhardt, and J. D. Harvey, "Polarization modulation instability in weakly birefringent fibers," *Opt. Lett.*, vol. 20, pp. 866–868, Apr. 1995.
[16] F. Lu and W. Knox, "Low noise wavelength conversion of femtosecond pulses with dispersion micro-managed holey fibers," *Opt. Exp.*, vol. 13, pp. 8172–8178, Oct. 2005.
[17] V. V. Lozovoy, I. Pastirk, and M. Dantus, "Multiphoton intrapulse interference. IV. Ultrashort laser pulse spectral phase characterization and compensation," *Opt. Lett.*, vol. 29, pp. 775–777, Apr. 2004.
[18] B. Xu, J. M. Gunn, J. M. D. Cruz, V. V. Lozovoy, and M. Dantus, "Quantitative investigation of the multiphoton intrapulse interference phase scan method for simultaneous phase measurement and compensation of femtosecond laser pulses," *J. Opt. Soc. Am. B*, vol. 23, pp. 750–759, Apr. 2006.
[19] B. Metzger, A. Steinmann, and H. Giessen, "High-power widely tunable sub-20fs Gaussian laser pulses for ultrafast nonlinear spectroscopy," *Opt. Exp.*, vol. 19, pp. 24354–24360, Nov. 2011.
[20] N. Karasawa, L. Li, A. Suguro, H. Shigekawa, R. Morita, and M. Yamashita, "Optical pulse compression to 5.0 fs by use of only a spatial light modulator for phase compensation," *J. Opt. Soc. Am. B*, vol. 18, pp. 1742–1746, Nov. 2001.
[21] B. Schenkel, R. Paschotta, and U. Keller, "Pulse compression with supercontinuum generation in microstructure fibers," *J. Opt. Soc. Am. B*, vol. 22, pp. 687–693, Mar. 2005.
[22] B. von Vacano, T. Buckup, and M. Motzkus, "Shaper-assisted collinear SPIDER: Fast and simple broadband pulse compression in nonlinear microscopy," *J. Opt. Soc. Am. B*, vol. 24, pp. 1091–1100, May 2007.
[23] A. M. Weiner, "Femtosecond pulse shaping using spatial light modulators," *Rev. Sci. Instrum.*, vol. 71, no. 5, pp. 1929–1960, May 2000.
[24] Y. Liu, H. Tu, W. A. Benalcazar, E. J. Chaney, and S. A. Boppart, "Multimodal nonlinear microscopy by shaping a fiber supercontinuum from 900 to 1160 nm," *IEEE J. Sel. Top. Quantum Electron.*, vol. 18, no. 3, pp. 1209–1214, May 2012.
[25] J. M. Stone and J. C. Knight, "Visibly "white" light generation in uniform photonic crystal fiber using a microchip laser," *Opt. Exp.*, vol. 16, pp. 2670–2675, Feb. 2008.
[26] J. C. Travers, "Blue extension of optical fibre supercontinuum generation," *J. Opt.*, vol. 12, art. no. 113001, Oct. 2010.
[27] K. L. Corwin, N. R. Newbury, J. M. Dudley, S. Coen, S. A. Diddams, K. Weber, and R. S. Windeler, "Fundamental noise limitations to supercontinuum generation in microstructure fiber," *Phys. Rev. Lett.*, vol. 90, art. no. 113904, Mar. 2003.
[28] U. Møller, S. T. Sørensen, C. Jakobsen, J. Johansen, P. M. Moselund, C. L. Thomsen, and O. Bang, "Power dependence of supercontinuum noise in uniform and tapered PCFs," *Opt. Exp.*, vol. 20, pp. 2851–2857, Jan. 2012.
[29] D. Solli, C. Ropers, P. Koonath, and B. Jalali, "Optical rogue waves," *Nature*, vol. 450, pp. 1054–1057, Dec. 2007.
[30] M. Erkintalo, G. Genty, and J. M. Dudley, "Rogue-wave-like characteristics in femtosecond supercontinuum generation," *Opt. Lett.*, vol. 34, pp. 2468–2470, Aug. 2009.
[31] J. M. Dudley, G. Genty, and B. J. Eggleton, "Harnessing and control of optical rogue waves in supercontinuum generation," *Opt. Exp.*, vol. 16, pp. 3644–3651, Mar. 2008.
[32] Z. Zhu and T. G. Brown, "Polarization properties of supercontinuum spectra generated in birefringent photonic crystal fibers," *J. Opt. Soc. Am. B*, vol. 21, pp. 249–257, Feb. 2004.
[33] J. Ramsay, S. Dupont, and S. R. Keiding, "Pulse-to-pulse noise reduction in infrared supercontinuum spectroscopy: Polarization and amplitude fluctuations," *Laser Phys. Lett.*, vol. 11, art. no. 095702, Jul. 2014.
[34] G. Genty, M. Surakka, J. Turunen, and A. T. Friberg, "Complete characterization of supercontinuum coherence," *J. Opt. Soc. Am. B*, vol. 28, pp. 2301–2309, Sep. 2011.
[35] G. Genty, J. M. Dudley, and B. J. Eggleton, "Modulation control and spectral shaping of optical fiber supercontinuum generation in the picosecond regime," *Appl. Phys. B*, vol. 94, pp. 187–194, Nov. 2008.
[36] D. R. Solli, C. Ropers, and B. Jalali, "Active control of rogue waves for stimulated supercontinuum generation," *Phys. Rev. Lett.*, vol. 101, pp. 18–21, Dec. 2008.
[37] P. M. Moselund, M. H. Frosz, C. L. Thomsen, and O. Bang, "Back-seeding of higher order gain processes in picosecond supercontinuum generation," *Opt. Exp.*, vol. 16, pp. 11954–11968, Aug. 2008.
[38] A. Kudlinski, B. Barviau, A. Leray, C. Spriet, L. Héliot, and A. Mussot, "Control of pulse-to-pulse fluctuations in visible supercontinuum," *Opt. Exp.*, vol. 18, pp. 27445–27454, Dec. 2010.
[39] Y. Liu, H. Tu, and S. A. Boppart, "Wave-breaking-extended fiber supercontinuum generation for high compression ratio transform-limited pulse compression," *Opt. Lett.*, vol. 37, pp. 2172–2174, Jun. 2012.

Authors' biographies not available at the time of publication.